FERMION MASS EFFECTS AT LINEAR COLLIDERS * **

KAROL KOŁODZIEJ

Institute of Physics, University of Silesia
Uniwersytecka 4, 40-007 Katowice, Poland
e-mail: kolodzie@us.edu.pl

(Received October 19, 2001)

A few physical examples are discussed which illustrate a role of fermion masses in the Standard Model predictions for reactions which will be measured at future linear colliders. Taking into account nonzero fermion masses is important not only in the context of the Higgs boson, or the top quark pair production and decay. The mass effects may also become numerically sizable for reactions involving light fermion flavours only. It is interesting that the mass effects do not always disappear in the presence of cuts. In some situations, the cuts may even enlarge the mass effect or make it inverse, *i.e.* stronger for lighter fermion flavours than for heavier ones.

PACS numbers: 12.15.–y, 13.40.Ks, 14.65.Ha

1. Introduction

Tests of the non Abelian structure of the Standard Model (SM) and mass generation mechanism at future e^+e^- linear colliders like TESLA [1], NLC [2] or JLC [3] require precise theoretical predictions for such SM processes as W-pair production, Higgs boson production or top quark pair production, see, *e.g.*, [4]. As the particles of interest will be reconstructed in detectors through their decay products, it is crucial to know the SM predictions for reactions containing four, six, or even more fermions in the final state

$$e^+e^- \to 4f, 6f, \ldots . \tag{1}$$

* Presented at the XXV International School of Theoretical Physics "Particles and Astrophysics — Standard Models and Beyond", Ustroń, Poland, September 10–16, 2001.

** Work supported in part by the Polish State Committee for Scientific Research (KBN) under contract no. 2 P03B 004 18 and by the European Commission's 5-th Framework contract HPRN-CT-2000-00149.

Such reactions usually receive contributions from a large number of Feynman diagrams and obtaining reliable theoretical predictions for them within the SM is a complicated task already at the Born level. As some experiments planned at future linear colliders, especially at a high luminosity collider like TESLA [1], are aiming at the precision of 0.1%, it is necessary to include radiative corrections in the SM theoretical predictions. Up to now there is no calculation of the complete $\mathcal{O}(\alpha)$ virtual corrections to any specific channel of (1). However, leading radiative effects to the four fermion channels of reactions (1) containing a pair of W bosons in the intermediate state have been calculated within the approach usually referred to as a double pole approximation [5, 6]. See also [7]. Concerning real photonic corrections to the four fermion reactions, the situation looks much better. There are a few program packages which allow to calculate cross sections of

$$e^+e^- \to 4f\gamma \tag{2}$$

for any specific four fermion final state that is possible in the framework of the SM. For a systematic review and references see, *e.g.*, [8].

In order to facilitate computations, masses of the initial and final state fermions are very often neglected in reactions (1). Although, it is clear that neglecting the fermion masses sometimes causes problems such as, for example, collinear divergences, the $\sim 1/s_{f\bar{f}}$ divergence related to emission of a virtual photon decaying into a massless fermion–antifermion pair, or the lack of consistency in implementing the Higgs boson exchange. In the massless limit, it is also not possible to make consistent predictions for production of heavy fermion flavours. It is clear that most of these problems disappear if cuts, which are anyway present in any realistic experimental setup, are imposed. In the presence of cuts, the fermion masses should play no role for most physical observables. In the following, a few physical examples will be discussed which clearly show that it need not always be the case and that the fermion mass effects may be relevant not only in the context of Higgs boson production and decay, or production and decay of heavy flavour quarks, as for example in the reaction

$$e^+e^- \to \bar{t}t \to 6f\,, \tag{3}$$

but also for reactions involving light flavours, as for example radiative processes (2).

Numerical results for fermion mass effects are discussed in Section 2 and the summary of the paper is given in Section 3.

2. Numerical results

Numerical results presented in this section have been obtained in earlier works: the results for four fermion processes of (1) and the corresponding bremsstrahlung reactions (2) in [9], the results for processes containing a single on-mass-shell top quark in [10], and the results for the top quark pair production and decay into 6 fermions (3) in [11]. Therefore, for the details of calculation and specific values of physical parameters, an interested reader should refer to [9–11] and earlier works, [12] and [13]. For convenience of the reader one should only remind that constant widths of unstable particles, Γ_W, Γ_Z, Γ_H and Γ_t are introduced through the complex mass parameters

$$M_V^2 = m_V^2 - im_V\Gamma_V\,, \quad V = W, Z, H\,, \quad M_t = m_t - \frac{i\Gamma_t}{2} \tag{4}$$

in the corresponding propagators and, if not stated otherwise, the electroweak mixing parameter

$$\sin^2\theta_W = 1 - \frac{m_W^2}{m_Z^2} \tag{5}$$

is kept real. This kind of parametrization is usually referred to as the Fixed-Width Scheme (FWS). It is also possible to define $\sin^2\theta_W$ in terms of the complex masses of Eqs. (4) as

$$\sin^2\theta_W = 1 - \frac{M_W^2}{M_Z^2} \tag{6}$$

which is usually called the Complex-Mass Scheme (CMS). The CMS has the advantage that it satisfies the Ward identities [14]. However, the fact that (6) makes some of the SM couplings complex quantities may become a source of discomfort. In the FWS, on the other hand, all the couplings remain real, but only the electromagnetic gauge invariance is satisfied provided that Γ_t and the other fermion widths are vanishing. It should be stressed at this point, that for vanishing fermion widths, electromagnetic gauge invariance is preserved with non-zero fermion masses and with the gauge boson widths Γ_W and Γ_Z treated as independent parameters. If a non-vanishing top quark width is introduced through the substitution (4), electromagnetic gauge invariance gets violated. However, as it will be shown in Section 2.2, the violation of the gauge symmetry does not lead to significant effects for the total cross sections of reactions (2) containing a top quark in the final state.

In the following Tables, the numbers in parenthesis are standard deviations of the Monte Carlo (MC) integration, which show an uncertainty of the last decimals. The standard deviation of the multichannel MC integration routine is obtained as a sum of the standard deviations calculated by VEGAS [15] for individual channels. This gives a more conservative estimate of the error than for example adding up partial errors in quadrature.

2.1. Four fermion reactions and the bremsstrahlung

In this subsection, the mass effects in four fermion reactions (1) and the corresponding bremsstrahlung processes (2) will be discussed.

The results for selected four-fermion channels of reactions (1) and (2) are collected in Tables I–III, where total cross sections at two centre of mass energies, $\sqrt{s} = 200$ GeV and $\sqrt{s} = 500$ GeV, with cuts are shown. The cuts are defined, as in [8], by

$$\begin{aligned} &\cos\theta(l,\text{beam}) \leq 0.985, \quad \theta(\gamma,l) > 5^\circ, \quad E_\gamma > 1 \text{ GeV}, \quad m(q,q') > 10 \text{ GeV}, \\ &\cos\theta(\gamma,\text{beam}) \leq 0.985, \quad \theta(\gamma,q) > 5^\circ, \quad E_l > 5 \text{ GeV}, \end{aligned} \tag{7}$$

where l, q, γ, and "beam" denote charged leptons, quarks, photons, and the beam (electrons or positrons), respectively, and $\theta(i,j)$ the angles between the particles i and j in the c.m.s. Furthermore, $m(q,q')$ denotes the invariant mass of a quark pair qq'.

In Tables I and II, the results for the four fermion channels of (1) and bremsstrahlung reactions (2) corresponding to the W-pair and the single W signal are shown. These channels are usually classified as charged current reactions. One sees that, both in Tables I and II, the cross sections of purely hadronic channels are about a factor 3 bigger than the cross sections of semi-leptonic channels and the latter are a factor 3 bigger than the cross sections of purely leptonic reactions. This reflects the naive counting of the colour degrees of freedom. This somewhat general rule is obviously violated in reactions which receive contributions from the gluon or t-channel photon and Z exchange. Except for the channels containing heavy quarks, t and b, for lighter flavors, the fermion mass effects are not big. However, for individual channels, they are of the order of a few per cent, as it has been already pointed out in [13]. It is amazing that the mass effect is inverse for $e^+e^- \to u\bar{d}d\bar{u}$ and $e^+e^- \to c\bar{s}s\bar{c}$. It is not the Higgs boson exchange, but rather cuts of Eqs. (7), which are responsible for this inversion. The cuts reduce contribution of the s-channel Feynman diagrams to $e^+e^- \to u\bar{d}d\bar{u}$ to much larger extent than to $e^+e^- \to c\bar{s}s\bar{c}$, as the cut on invariant mass of the quark pair restricts the phase space much more severely for lighter quarks than for heavier ones. Without the cuts, the cross section of $e^+e^- \to u\bar{d}d\bar{u}$ becomes bigger than that of $e^+e^- \to c\bar{s}s\bar{c}$, as expected.

TABLE I

Cross sections in fb of (1) and (2) at $\sqrt{s} = 200$ GeV and $\sqrt{s} = 500$ GeV for several four-fermion final states corresponding to the W-pair signal. The cuts are those of Eqs. (7).

Final	$\sqrt{s} = 200$ GeV		$\sqrt{s} = 500$ GeV	
state	σ	σ_γ	σ	σ_γ
$u\bar{d}\mu^-\bar{\nu}_\mu$	630.65(31)	70.547(83)	211.11(13)	23.601(46)
$c\bar{s}\tau^-\bar{\nu}_\tau$	629.93(31)	67.279(72)	210.87(13)	23.077(43)
$t\bar{b}\mu^-\bar{\nu}_\mu$	—	—	58.88(30)	9.467(60)
$c\bar{s}d\bar{u}$	1838.6(1.4)	172.74(28)	749.07(50)	68.34(23)
$t\bar{b}d\bar{u}$	—	—	177.8(1.9)	25.55(42)
$\nu_\tau\tau^+\mu^-\bar{\nu}_\mu$	205.88(15)	25.784(44)	60.762(62)	7.842(23)
$u\bar{d}d\bar{u}$	1921.4(7)	188.19(46)	780.66(25)	74.99(28)
$c\bar{s}s\bar{c}$	1925.7(8)	184.07(46)	782.62(28)	73.46(25)
$t\bar{b}b\bar{t}$	—	—	0.85519(56)	0.073748(78)
$\nu_\mu\mu^+\mu^-\bar{\nu}_\mu$	218.91(19)	28.232(55)	63.933(70)	8.475(26)
$\nu_\tau\tau^+\tau^-\bar{\nu}_\tau$	214.94(20)	26.280(50)	63.468(74)	8.299(20)
$\nu_e e^+ e^-\bar{\nu}_e$	259.55(31)	32.012(93)	195.22(42)	24.85(14)

TABLE II

Cross sections in fb of (1) and (2) at $\sqrt{s} = 200$ GeV and $\sqrt{s} = 500$ GeV for different four-fermion final states corresponding to the single W signal. The cuts are those of Eqs. (7).

Final	$\sqrt{s} = 200$ GeV		$\sqrt{s} = 500$ GeV	
state	σ	σ_γ	σ	σ_γ
$u\bar{d}e^-\bar{\nu}_e$	661.68(40)	72.95(10)	354.06(27)	38.876(88)
$c\bar{s}e^-\bar{\nu}_e$	661.42(40)	71.84(10)	353.91(27)	38.371(88)
$t\bar{b}e^-\bar{\nu}_e$	—	—	58.54(65)	9.43(16)
$\nu_\mu\mu^+e^-\bar{\nu}_e$	216.29(21)	27.473(57)	107.34(14)	13.677(43)
$\nu_\tau\tau^+e^-\bar{\nu}_e$	216.13(21)	26.709(55)	107.25(13)	13.471(42)

The results for several neutral current channels of reactions (1) and (2) are shown in Table III. The cross sections of Table III are typically much smaller then those of Tables I and II. Mass effects on the other hand are bigger. The stronger dependence on fermion masses can be explained as follows. The neutral-current reactions are dominated by the s-channel Feynman diagrams which contain the propagator of a photon decaying into a fermion pair. This causes a $\sim 1/s_{ff'}$ behaviour of the matrix element squared and results in a relatively high sensitivity to the fermion pair threshold $s_{ff'} = (m_f + m_{f'})^2$. There is a relatively big effect for charged lepton pairs $\mu^+\mu^-$, $\tau^+\tau^-$ and much smaller effect for quark pairs, except for $\bar{t}t$, of course. This is related to the fact that there is no cut on the invariant mass of a charge lepton pair imposed in Eqs. (7). Again an inverse mass effect in some channels, especially those containing a neutrino pair, can be observed. The cross section of $e^+e^- \to \bar{d}d\bar{\nu}_e\nu_e$ is bigger than that of $e^+e^- \to \bar{u}u\bar{\nu}_e\nu_e$ although a mass of the d-quark used in the calculation, $m_d = 9$ MeV, is almost twice as big as that of the u-quark, $m_u = 5$ MeV. The inverse mass effect is caused by the invariant mass cut $m(q,q') > 10$ GeV of Eqs. (7), which is more restrictive for lighter fermion pairs than for heavier ones and by the fact that there is neither invariant mass nor angular cut on a neutrino-pair. It is seen that the mass effects depend on cuts. They may be different for different choices of cuts.

TABLE III

Cross sections in fb, for different neutral current four-fermion final states. The cuts are those of Eqs. (7).

Final	$\sqrt{s} = 200$ GeV		$\sqrt{s} = 500$ GeV	
state	σ	σ_γ	σ	σ_γ
$\bar{u}u\mu^+\mu^-$	27.341(30)	4.874(13)	6.855(10)	1.5630(62)
$\bar{c}c\tau^+\tau^-$	19.560(16)	3.4407(92)	6.0566(68)	1.3922(48)
$\bar{d}d\bar{\nu}_e\nu_e$	26.820(20)	1.6916(23)	57.03(27)	5.731(36)
$\bar{b}b\bar{\nu}_e\nu_e$	31.346(28)	1.8819(33)	128.31(65)	12.59(12)
$\bar{d}d\bar{s}s$	79.658(95)	9.77(11)	29.812(39)	4.159(34)
$\bar{d}d\bar{b}b$	82.486(87)	10.436(86)	37.435(39)	5.363(26)
$\bar{d}d\bar{d}d$	39.173(32)	4.791(20)	14.758(15)	2.0706(76)
$\bar{s}s\bar{s}s$	39.167(32)	4.810(20)	14.767(15)	2.0769(76)
$\bar{b}b\bar{b}b$	41.667(24)	5.217(14)	22.242(14)	3.2142(67)

Comparing the channels containing a $\bar{b}b$- or $\bar{c}c$-pair with those containing lighter quark flavors in Table III, one sees a clear signal of the Higgs-strahlung reaction $e^+e^- \to ZH$, especially at $\sqrt{s} = 500$ GeV, which exceeds the ZH production threshold for a Higgs boson mass of 115 GeV. In case of $e^+e^- \to \bar{b}b\bar{\nu}_e\nu_e$ and $e^+e^- \to \bar{c}c\bar{\nu}_e\nu_e$, also a signal of a W^+W^- fusion mechanism of the Higgs boson production is visible. For the final state containing a $\bar{b}b$-pair, the Higgs signal is seen already at $\sqrt{s} = 200$ GeV and it becomes much more pronounced at $\sqrt{s} = 500$ GeV.

2.2. Production of heavy flavours in $e^+e^- \to 4f$

In this subsection, production of heavy flavours, in the four fermion channel of reaction (1) will be discussed.

Consider the production of a $t\bar{t}$-quark pair, $e^+e^- \to t\bar{t}$ and let the anti-top quark $\bar{t}$ decay into a final state possible in the framework of the SM, *i.e.*, consider reactions

$$e^+e^- \to t\bar{b}f\bar{f}', \tag{8}$$

where $f = e^-, \mu^-, \tau^-, d, s$ and $f' = \nu_e, \nu_\mu, \nu_\tau, u, c$, respectively, taking into account the complete set of the Feynman graphs which contribute to the specific final state at the tree level. As it has been already pointed out in the Introduction, introducing the nonzero top quark width through substitution (4) violates the electromagnetic gauge invariance. Therefore, in order to test reliability of the predictions for reaction (8), the calculation has been performed in the arbitrary linear R_ξ gauge [10].

The results for the cross sections of $e^+e^- \to t\bar{b}\mu^-\bar{\nu}_\mu$ at different centre of mass energies obtained in different schemes and gauges: the Complex-Mass Scheme (CMS), Fixed Width Scheme (FWS), Unitary Gauge (UG) and Feynman Gauge (FG) are shown in Table IV. Numerical integration has been performed over the full four particle phase space without any cuts. One can see that the results in Table IV hardly depend on the gauge choice both in the CMS and FWS. Actually, they nicely agree with each other within one standard deviation of the MC integration. It should be stressed at this point that the transition between the two gauges, FG and UG, has been performed numerically by varying the gauge parameter ξ by 16 orders of magnitude, from $\xi = 1$ to $\xi = 10^{16}$.

In Table V, the results for $e^+e^- \to t\bar{b}e^-\bar{\nu}_e$ obtained in the CMS and in two different gauges, UG and FG, for two different cuts on the electron angle with respect to the beam $\theta(e^-, \text{beam})$ are presented. There is rather small dependence on the angular cut for the energies presented in Table V. From a comparison with the corresponding numbers of Table IV, one can infer that the t-channel Feynman graphs of reaction $e^+e^- \to t\bar{b}e^-\bar{\nu}_e$ do not contribute much to the total cross section in the presence of the cut

TABLE IV

Cross sections in fb of $e^+e^- \to t\bar{b}\mu^-\bar{\nu}_\mu$ at different centre of mass energies in different schemes, CMS and FWS, and gauges, UG and FG. The numbers in parenthesis show the uncertainty of the last decimals.

$\sqrt{s}$ (GeV)	$\sigma^{\rm UG}_{\rm CMS}$	$\sigma^{\rm FG}_{\rm CMS}$	$\sigma^{\rm UG}_{\rm FWS}$	$\sigma^{\rm FG}_{\rm FWS}$
340	0.7837(4)	0.7837(4)	0.7839(4)	0.7840(4)
360	41.27(10)	41.27(10)	41.28(10)	41.29(10)
500	60.06(13)	60.04(13)	59.75(30)	59.90(29)
2000	5.59(3)	5.56(3)	5.51(7)	5.51(8)

on the final electron angle. When the cut is further reduced, so that the denominator of the t-channel photon propagator becomes of the order of the squared electron mass, the dependence on gauge becomes substantial and results are meaningless.

TABLE V

Cross sections in fb of $e^+e^- \to t\bar{b}e^-\bar{\nu}_e$ in the CMS in two different gauges, UG and FG, and for two different cuts on the electron angle with respect to the beam.

$\sqrt{s}$	$5^\circ < \theta(e^-, \text{beam}) < 175^\circ$		$1^\circ < \theta(e^-, \text{beam}) < 179^\circ$	
(GeV)	$\sigma^{\rm UG}_{\rm CMS}$	$\sigma^{\rm FG}_{\rm CMS}$	$\sigma^{\rm UG}_{\rm CMS}$	$\sigma^{\rm FG}_{\rm CMS}$
340	0.7993(4)	0.7993(4)	0.8251(4)	0.8253(4)
360	41.21(11)	41.20(11)	41.32(8)	41.32(8)
500	59.78(15)	59.75(15)	60.16(15)	60.19(15)
2000	6.81(3)	6.82(3)	7.97(3)	8.00(3)

The results for the channels of reaction (8) which do not contain electron in the final state are shown in Table VI. They were obtained in the CMS and unitary gauge. Again, as expected, the results for the purely hadronic channels are a factor 3 bigger than those of the semileptonic channels. There is practically no dependence on masses of lighter flavours in Table VI.

The dependence of the total cross section of $e^+e^- \to t\bar{b}\mu^-\bar{\nu}_\mu$ on the top quark width Γ_t is shown in Table VII. It can be seen that the cross section at $\sqrt{s} = 360$ GeV, *i.e.* just above the $t\bar{t}$ threshold, is almost exactly

TABLE VI

Cross sections in the CMS in fb of different channels of reaction (8) not containing a final state electron.

Channel of reaction (8)	$\sqrt{s}$ (GeV)			
	340	360	500	2000
$e^+e^- \to t\bar{b}\mu^-\bar{\nu}_\mu$	0.7837(4)	41.3(1)	59.8(3)	5.42(7)
$e^+e^- \to t\bar{b}\tau^-\bar{\nu}_\tau$	0.7831(4)	41.2(1)	59.6(3)	5.47(7)
$e^+e^- \to t\bar{b}d\bar{u}$	2.351(1)	123.8(3)	179.9(9)	16.3(2)
$e^+e^- \to t\bar{b}s\bar{c}$	2.350(1)	123.8(3)	178.9(9)	16.7(2)

TABLE VII

Cross sections in fb of $e^+e^- \to t\bar{b}\mu^-\bar{\nu}_\mu$ for different values of the top quark width. The calculation has been performed in the CMS and UG.

$\sqrt{s}$ (GeV)	Γ_t (GeV)		
	1.5	1.6	1.7
340	0.7837(4)	0.7832(3)	0.7830(3)
360	41.27(10)	38.65(7)	36.31(6)
500	60.06(13)	56.37(13)	53.13(12)
2000	5.59(3)	5.30(2)	5.09(2)

proportional to $1/\Gamma_t$. This kind of dependence holds also at $\sqrt{s} = 500$ GeV, which is already much above the threshold and it survives almost unaltered at $\sqrt{s} = 2$ TeV. It means that the cross section of $e^+e^- \to t\bar{b}\mu^-\bar{\nu}_\mu$ is well approximated by the resonant $\bar{t}$ production and its subsequent decay. This kind of dependence offers a new way of measurement of the top quark width alternative to the measurement based on the shape of the $t\bar{t}$ threshold [16].

2.3. Production and decay of a $t\bar{t}$-pair

As measurements of the top quark physical characteristics, in particular its static properties such as magnetic and electric dipole moments, will be performed at high energies, much above the $t\bar{t}$ threshold, it is crucial to know off-resonance background contributions to any specific 6 fermion decay channel and to estimate the effects related to the off-shellness of the $t\bar{t}$-pair. Therefore, in this subsection, the 6 fermion reactions of the form

$$e^+e^- \to bf_1\bar{f}_1'\bar{b}f_2\bar{f}_2', \tag{9}$$

where $f_1 = \nu_\mu, \nu_\tau, u, c$, $f_2 = \mu^-, \tau^-, d, s$, and f_1', f_2' are the corresponding weak isospin partners of f_1, f_2, $f_1' = \mu^-, \tau^-, d, s$, $f_2' = \nu_\mu, \nu_\tau, u, c$, are discussed. For the sake of simplicity, it is assumed that the actual values of f_1 and f_2' are different from each other, and that neither f_1' nor f_2 is an electron. The complete lowest order SM results for reaction (9) are compared with the results obtained in a few different approximations: the double resonance approximation for W bosons

$$e^+e^- \to bW^{+*}\bar{b}W^{-*} \to bf_1\bar{f}_1'\bar{b}f_2\bar{f}_2', \tag{10}$$

where only those 61 Feynman diagrams are taken into account which contribute to $e^+e^- \to bW^+\bar{b}W^-$ with the W bosons being off-mass-shell, the double resonance approximation for a t- and $\bar{t}$-quark

$$e^+e^- \to t^*\bar{t}^* \to bf_1\bar{f}_1'\bar{b}f_2\bar{f}_2' \tag{11}$$

with only two 'signal' diagrams contributing and, finally, with 3 different narrow width approximations: for the W bosons, top and antitop quarks, and a single top quark discussed already in Section 2.2.

The cross section of reaction (10) in the narrow W width approximation is given by

$$\sigma_{bW^+\bar{b}W^-} = \sigma(e^+e^- \to bW^+\bar{b}W^-)\, \Gamma\left(W^+ \to f_1\bar{f}_1'\right) \frac{\Gamma\left(W^- \to f_2\bar{f}_2'\right)}{\Gamma_W^2}. \tag{12}$$

Similarly, the cross section of reaction (11) in the narrow width approximation for the top and antitop reads

$$\sigma_{t\bar{t}} = \sigma(e^+e^- \to t\bar{t})\, \Gamma\left(t \to bf_1\bar{f}_1'\right) \frac{\Gamma\left(\bar{t} \to \bar{b}f_2\bar{f}_2'\right)}{{\Gamma_t}^2}. \tag{13}$$

Finally, in the approximation where only the top quark is put on its mass shell, the cross section is given by

$$\sigma_{t\bar{b}f_2\bar{f}_2'} = \sigma(e^+e^- \to t\bar{b}f_2\bar{f}_2') \frac{\Gamma\left(t \to bf_1\bar{f}_1'\right)}{\Gamma_t}. \tag{14}$$

The lowest order SM total cross sections of the semileptonic channel $e^+e^- \to b\nu_\mu\mu^+\bar{b}d\bar{u}$ of reaction (9) at different c.m.s. energies typical for future linear colliders are shown in Table VIII. The complete lowest order result σ, the approximation of Eq. (10) $\sigma_{bW^*\bar{b}W^*}$, the narrow W width approximation of Eq. (12) $\sigma_{bW\bar{b}W}$, the approximation of Eq. (11) $\sigma_{t^*\bar{t}^*}$, the narrow width approximation of Eq. (13) for a top and an antitop quark $\sigma_{t\bar{t}}$ and the narrow width approximation for a top quark of Eq. (14) $\sigma_{t\bar{b}d\bar{u}}$ have been all obtained in FWS. The SM tree level analytic expression for the partial widths of the W boson and the experimental value of total W width Γ_W have been used in Eq. (12). Similarly, the SM tree level analytic expression for the partial widths of the t quark in the zero fermion mass approximation [17] and the top width $\Gamma_t = 1.5$ GeV have been used in Eqs. (13) and (14). The use of these particular values of Γ_W and Γ_t in Eqs. (12)–(14) is preferred in the comparison because the same values have been used in substitutions of Eq. (4).

TABLE VIII

The lowest order SM total cross sections of $e^+e^- \to b\nu_\mu\mu^+\bar{b}d\bar{u}$ in fb at different c.m.s. energies in GeV: the complete lowest order result σ, the approximation of Eq. (10) $\sigma_{bW^*\bar{b}W^*}$, the narrow W width approximation of Eq. (12) $\sigma_{bW\bar{b}W}$, the approximation of Eq. (11) $\sigma_{t^*\bar{t}^*}$, the narrow width approximation of Eq. (13) for a top and an antitop quark $\sigma_{t\bar{t}}$ and the narrow width approximation for top quark of Eq. (14) $\sigma_{t\bar{b}d\bar{u}}$. The number in parenthesis show the uncertainty of the last decimal.

$\sqrt{s}$	σ	$\sigma_{bW^*\bar{b}W^*}$	$\sigma_{bW\bar{b}W}$	$\sigma_{t^*\bar{t}^*}$	$\sigma_{t\bar{t}}$	$\sigma_{t\bar{b}d\bar{u}}$
340	1.162(7)	0.681(6)	0.671(1)	0.3521(2)	—	0.2546(3)
360	13.64(2)	13.224(8)	13.618(8)	12.79(1)	13.875	13.42(1)
500	20.48(9)	20.17(1)	20.79(1)	19.06(1)	19.223	19.51(3)
800	10.61(4)	10.46(3)	10.75(1)	9.181(5)	8.918	9.47(1)
1000	7.35(4)	7.33(4)	7.54(1)	6.171(4)	5.862	6.390(7)
2000	2.43(2)	2.48(3)	2.48(1)	1.847(2)	1.510	1.822(2)

As the cross section of the 6 fermion reaction $e^+e^- \to b\nu_\mu\mu^+\bar{b}d\bar{u}$ is nonzero below the $t\bar{t}$-pair production threshold, the precision of measurements at the threshold may be affected. This background can be probably easily reduced by imposing cuts, which unfortunately will reduce the $t\bar{t}$ signal, too. Close to threshold, at $\sqrt{s} = 360$ GeV, the relative difference between σ and the narrow width approximation $\sigma_{t\bar{t}}$ is about -1.5%, whereas in the continuum the difference becomes bigger, amounting to 7%

at $\sqrt{s} = 500$ GeV and 19% at $\sqrt{s} = 800$ GeV. At higher energies, the difference between σ and $\sigma_{t\bar{t}}$ becomes so large that approximation (13) does not make sense any more. Comparison of approximated results $\sigma_{bW^*\bar{b}W^*}$ and $\sigma_{bW\bar{b}W}$ with the complete result σ shows that approximations of Eqs. (10) and (12) are relatively much better in a range of the c.m.s. energy from 360 GeV to 2 TeV.

The pure off-shellness effects of the $t\bar{t}$-pair can be regarded as the difference between approximations $\sigma_{t^*\bar{t}^*}$ of Eq. (11) and $\sigma_{t\bar{t}}$ of Eq. (13). They are plotted in Fig. 1 as a function of the c.m.s. energy.

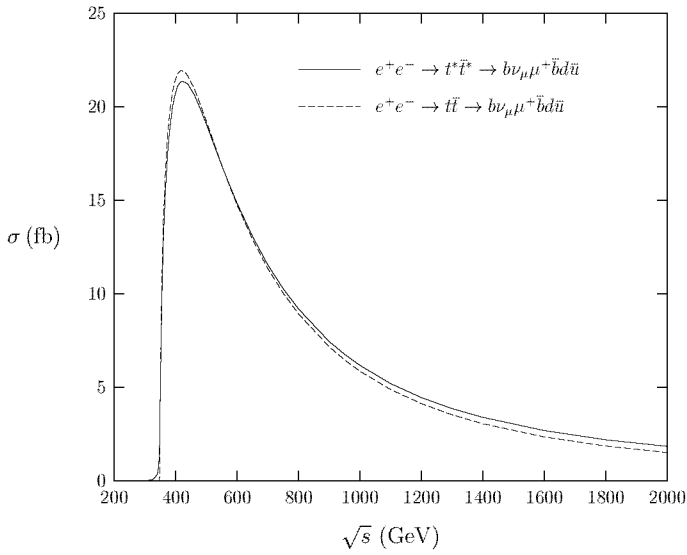

Fig. 1. Total cross sections of $e^+e^- \to b\nu_\mu\mu^+\bar{b}d\bar{u}$ in approximations of Eqs. (11) (solid line) and (13) (dashed line) as functions of the c.m.s. energy.

How the background nonresonant contributions may affect differential cross sections of (9) is illustrated in Fig. 2, where the differential cross sections $\mathrm{d}\sigma/\mathrm{d}\cos\theta$ of $e^+e^- \to b\nu_\mu\mu^+\bar{b}d\bar{u}$ at $\sqrt{s} = 360$ GeV are plotted versus cosine of the μ^+ (up going curves) and d (down going curves) angle with respect to the positron beam. The angular distributions obtained with the complete set of tree level Feynman diagrams differ substantially from the distributions based on approximations of Eqs. (10) and (11). The final state muon μ^+ (d-quark) goes more preferably in the direction of initial positron (electron) than it would follow from the approximated distributions based on Eqs. (10) and (11).

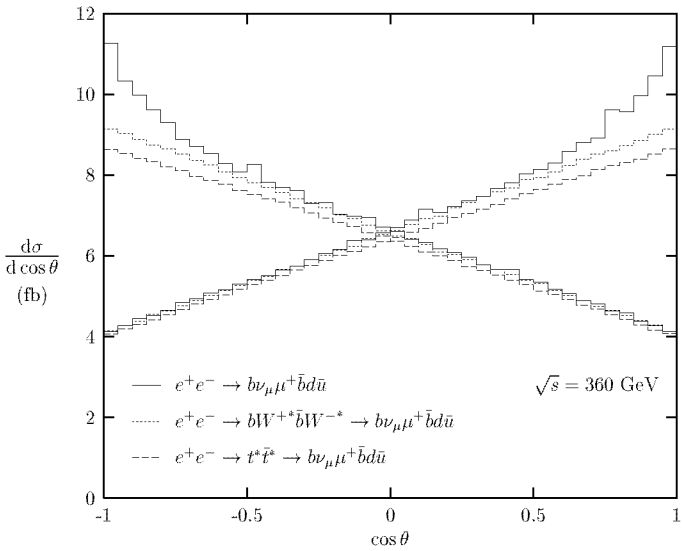

Fig. 2. Differential cross sections of $e^+e^- \to b\nu_\mu\mu^+\bar{b}d\bar{u}$ at $\sqrt{s} = 360$ GeV versus cosine of the μ^+ (up going curve) and d (down going curve) angle with respect to the positron beam.

3. Summary

A few physical examples have been discussed which illustrate a role of fermion masses in the SM predictions for reactions which will be measured at future linear colliders. Taking into account nonzero fermion masses is important not only in the context of the Higgs boson, or the top quark pair production and decay. The mass effects may also become numerically sizable for the bremsstrahlung reactions $e^+e^- \to 4f\gamma$ and for neutral current channels of the four fermion reactions $e^+e^- \to 4f$ involving light fermion flavours only. It is interesting that the mass effects do not always disappear in the presence of cuts. In some situations, the cuts may even enlarge the mass effect or make it inverse, *i.e.* stronger for lighter flavours than for heavier ones.

Whether or not the mass effects will play a role in the analysis of the future data depends mostly on luminosity of a linear collider. If one assumes a total integrated luminosity of 500 fb^{-1} they will certainly become relevant. Therefore it is better to keep nonzero fermion masses in theoretical predictions even for reactions involving light fermion flavours only, or test the massless fermion event generators against a massive one for each given set of cuts.

REFERENCES

[1] F. Richard, J.R. Schneider, D. Trines, A. Wagner, TESLA Technical Design Report Part I: Executive Summary, hep-ph/0106314.

[2] T. Abe *et al.*, [American Linear Collider Working Group Collaboration], SLAC-R-570 *Resource Book for Snowmass 2001.*

[3] K. Abe *et al.*, hep-ph/0109166.

[4] J.A. Aguilar-Saavedra *et al.* [ECFA/DESY LC Physics Working Group Collaboration], TESLA Technical Design Report Part III: Physics at an e^+e^- Linear Collider, hep-ph/0106315.

[5] A. Denner, S. Dittmaier, M. Roth, D. Wackeroth, *Nucl. Phys.* **B587**, 67 (2000).

[6] W. Płaczek, S. Jadach, M. Skrzypek, B.F.L. Ward, Z. Wąs, hep-ph/0012094.

[7] J. Fleischer, F. Jegerlehner, K. Kołodziej, G.J. van Oldenborgh, *Comput. Phys. Commun.* **85**, 29 (1995).

[8] M.W. Grünewald *et al.*, hep-ph/0005309.

[9] F. Jegerlehner, K. Kołodziej, hep-ph/0109290.

[10] A. Biernacik, K. Ciećkiewicz, K. Kołodziej, *Eur. Phys. J.* **C20**, 233 (2001).

[11] K. Kołodziej, hep-ph/0110063.

[12] F. Jegerlehner, K. Kołodziej, *Eur. Phys. J.* **C12**, 77 (2000).

[13] F. Jegerlehner, K. Kołodziej, *Eur. Phys. J.* **C20**, 227 (2001).

[14] A. Denner, S. Dittmaier, M. Roth, D. Wackeroth, *Nucl. Phys.* **B560**, 33 (1999).

[15] G.P. Lepage, *J. Comput. Phys.* **27**, 192 (1978).

[16] P. Comas, R. Miquel, M. Martinez, S. Orteu, in e^+e^- Collisions at TeV Energies: The Physics Potential, Proc. of the Workshop — Annecy, Gran Sasso, Hamburg, February 1995–September 1995, ed. P.M. Zerwas, DESY **96–123D**, 1 (1996).

[17] E. Boos, M. Dubinin, M. Sachwitz, H.J. Schreiber, *Eur. Phys. J.* **C16**, 269 (2000).